

Single-photon hot electron ionization of C₇₀

Åke Andersson,¹ Luca Schio,² Robert Richter,³ Michele Alagia,² Stefano Stranges,^{2,4} Piero Ferrari,⁵ Klavs Hansen,^{6,7,*} and Vitali Zhaunerchyk^{1,†}

¹*Department of Physics, University of Gothenburg, 41296 Gothenburg, Sweden*

²*IOM-CNR Tasc, SS-14, Km 163.5 Area Science Park, Basovizza, 34149 Trieste, Italy*

³*Elettra - Sincrotrone Trieste, Area Science Park, 34149 Basovizza, Trieste, Italy*

⁴*Dipartimento di Chimica e Tecnologie del Farmaco, Università Roma La Sapienza, Roma 00185, Italy Sapienza*

⁵*Quantum Solid-State Physics, Department of Physics and Astronomy, KU Leuven, 3001 Leuven, Belgium*

⁶*Lanzhou Center for Theoretical Physics, Key Laboratory of Theoretical Physics of Gansu Province and School of Physical Science and Technology, Lanzhou University, Lanzhou, Gansu 730000, China*

⁷*Center for Joint Quantum Studies and Department of Physics,*

School of Science, Tianjin University, 92 Weijin Road, Tianjin 300072, China

Gas phase C₇₀ molecules have been ionized with single photons of energies between 16 eV and 70 eV and the electron spectra measured with velocity map imaging in coincidence with the ions. The doubly ionized and unfragmented species was present at photon energies of 22 eV and up, and triply charged ions from 55 eV. The low kinetic energy parts of the spectra are explained with thermal emission of transient hot electrons. Deviations at high photon energies are used to determine a value for the initial electron equilibration time. We propose a generally applicable mechanism, named Resonance Ionization Shadowing, for the creation of hot electrons by absorption of above-threshold energy photons.

INTRODUCTION

The large separation in time scales for electronic and vibrational motion of the nuclei opens the possibility of an intermediate phase of transiently hot electrons in molecules and clusters. If present, this phase will exist between the time of the initial excitation of the electrons and the dissipation of the energy into vibrational motion. It tends to be manifested particularly clearly in finite systems, but has also been invoked in the description of the two-temperature model of solid surfaces exposed to short laser pulses [1].

In gas phase context it was introduced as the explanation of the Penning ionization yields of C₆₀ and C₇₀ in Ref. [2]. Soon after it was observed also to be present in C₆₀ upon excitation with multiple low energy photons from laser pulses of duration around 100 fs [3]. Subsequently, the phenomenon successfully explained ionization of sodium clusters with short pulse laser light [4–6]. Following this development, it has been seen for a number of different systems excited with short laser pulses, including C₇₀ [7] and a number of PAH (polycyclic aromatic) molecules [8].

The dynamics of multi-electron excited states involved in the phenomenon has been considered theoretically with different approaches in Refs. [9–11], in addition to the more phenomenological models used to summarize the experimental results. An integral part of this modeling when applied to molecules or clusters is the dissipation of the incoherent electronic excitation energy in the hot electron phase into the vibrational modes of the molecule. This coupling has been described in terms of a simple exponential decay of the excitation energy, involving a single parameter of dimension time, aptly named the coupling time. For some of the gas phase molecules studied, a proxy for this electron-phonon dissipation time has been measured by pump-probe experiments [6, 12]. In other cases it has been fitted from ion yield curves

for different clusters [13]. The values found range from a few hundred femtoseconds to a few picoseconds. The fastest dissipation occurs for C₆₀, with a time constant of 240 fs [13], and the slowest are the picosecond or longer times for sodium clusters [5]. With reservation for the still limited number of systems studied at this point, the data point to a dependence of the coupling time that correlates positively with the average vibrational period, as given by the vibrational frequencies of C₆₀ [14] and the bulk Debye temperature for sodium [5], although data from condensed phase nanoparticles show different trends [15]. Those data pertain to much lower temperatures than relevant here, though.

The correlation seen in gas phase particles suggests a dissipation mechanism based on internal conversion, i.e. with similarities to the energy dissipation in molecules after absorption of single photons. Experiments performed on thin films of C₇₀ have shown a very brief time window for equilibration, undetermined but below the pulse duration of 165 fs used in the experiments in Ref. [16]. Unfortunately it is not clear from these experiments if this time scale refers to the initial intra-electron equilibration or to the electron-phonon coupling time.

The initial electron equilibration in the creation of the hot electron phase has received much less attention experimentally than the final, dissipation stage. It is clearly a subject of interest for the possibility of single-photon ionization of larger classes of molecules. The observation of such single-photon hot electron ionization, already observed for C₆₀ [17], opens the possibility for studies of the mechanisms of absorption and initial dissipation of the energy. In addition to the general relevance for delineating the boundaries of the mechanism, single-photon excitation is also of interest in astrophysical context because molecular ions play an important role in the interstellar chemistry [18], and in particular for fullerenes because they have been identified in the interstellar medium.

The experiments reported here on C_{70} were motivated by the above questions. As an aside we mention that single-photon processes come with the additional and very attractive feature that they eliminate the uncertainty in energy that accompanies multi-photon processes previously used for studies of the subject. The experiments will also allow a test of the interpretation of the previous results on C_{60} in Ref. [17], using a molecule with almost equally well characterized and similar but still different properties.

The clearest experimental signature for these purposes remains the emission of electrons that are thermalized to the very high energies which characterize the hot electron phase. The emission of electrons that can be unambiguously assigned as hot electrons occurs between the initial excitation and the dissipation of energy into the vibrational motion. These distributions are unique to hot electron emission, and have the added experimental convenience that the spectra do not need to be measured time-resolved. However, ionization may also occur both before and after the creation of the hot electron phase. Either by direct ionization, which may remove enough energy by the departing electron to preempt the creation of the hot electron phase, or by thermionic emission after dissipation of the energy into the predominantly vibrational excitations of the equilibrium state.

The form of the thermal electron spectra is shaped by a number of factors [19]. One is the product of the emitted electrons' phase space and a flux factor in the form of the speed of the emitted electrons. These combine to give a factor proportional to the kinetic energy of the channel. A second factor is the cross section for the inverse (attachment) reaction. The third and last factor is the ratio of the level densities of the product and emitting molecules [13]. These factors enter the expression for the electron kinetic energy-resolved rate constants, which is identical to the one for the usual thermionic emission apart from the different level densities that describe the emitting systems in the two situations. The phase space and the speed factors combine to give the electron kinetic energy to the power one. For neutral or positively charged emitters the cross section of the inverse process of absorption is basically that of a Coulomb potential. In a classical calculation, which will be used here, it is proportional to the reciprocal of the electron energy, plus a constant (see ref. [13] for details). The ratio of level densities acts as an effective Boltzmann factor. The net result is that for neutral and positively charged emitters, the energy distributions calculated under these assumptions resemble Boltzmann factors with the effective temperatures given by the product microcanonical electron temperature, as discussed in [20]. For more information on the derivation of the expression, please see Ref. [21]. The very good consistency of several different experimentally measured quantities with the predictions derived from this description reported in [13] constitute a strong support of the modeling.

In addition to the Boltzmann-like shape of the spectrum, there are several other features that makes it distinct from the spectra originating either from direct ionization or from ther-

mal emission from completely equilibrated molecules, known as thermionic emission. A necessary feature of the spectra is that the velocity distributions of the emitted electrons must be spherically symmetric. This is a property shared with electrons emitted into single particle s -states, and for a single-photon excitation this could explain this symmetry, albeit not the Boltzmann shape. However, the energies of such electrons and indeed all electrons emitted from single-particle states move in parallel with the photon energy and will therefore have a different photon energy dependence than the hot electron spectra. Measurements at a few different photon energies are therefore sufficient to distinguish an origin of the relevant low energy part of the spectra as thermal or as emitted in a direct process.

A third possible origin of electrons, besides the hot electron emission and the direct ionization, is a regular thermionic process. There are two important differences between this type of process and hot electron emission. One is the effective temperature of the Boltzmann distribution. A standard thermionic emission process comes with an internal energy which renders the effective (microcanonical) temperature much lower than the hot electron emission. For fullerenes, for example, the thermionic emission temperature has been fitted to values around 3500 K from electron spectra measured with the velocity map imaging (VMI) technique also used in this work [22]. Although this is a very high temperature in many connections, the very fast emission required for the hot electron system requires much higher temperatures, on the order of 1 eV (= 11605 K) and higher [13]. The fitted temperature for the one photon hot electron ionization of C_{60} reported in [17] reached 1.6 eV, for example.

The other difference to hot electron ionization is the much longer time scale on which thermionic emission can be observed. Hot electron emission is limited to picosecond or sub-picosecond time scales. Thermionic emission, in contrast, will, for low excitation energies, extend to time scales that under some conditions can be detected as a several microsecond long tail on the mass peak in time-of-flight mass spectra [23] As a secondary signature, thermionic emission from neutral and cationic fullerenes is usually observed together with a substantial amount of fragmentation. Their absence here is only corroborative for the absence of thermionic emission, though.

For the doubly ionized species observed in the experiments here, two other possible channels should be considered. One is the direct double electron ionization. The electrons associated with prompt double ionization are characterized by a U-shaped electron kinetic energy distribution [24]. The steepness of these distributions depend on the relation between photon energy and the double ionization potential values.

Another possible channel is the emission of a second electron by regular thermionic emission. This process would occur after the excitation energy has been dissipated into the predominantly vibrationally excited equilibrium state. However, this is ruled out for two reasons. One is that the competing C_2 loss channel would dominate over thermionic emission by a

large factor. The second is that delayed emission is absent in the time-of-flight mass spectra for the double charged species.

In summary, the nature of the emission process is very well established, and displays the primary characteristic experimental features listed above. A number of further derived features can be found in [13, 25], where experiments on fullerenes and endohedral fullerenes exposed to short pulses of photons with energies below the ionization energy are described.

Apart from the initial Penning ionization study on C_{60} and C_{70} [2] and the one photon hot electron ionization study in Ref. [17], all of the experimental studies mentioned have been performed with short laser pulses of sub-threshold photon energies. Indeed, until recently, studies of the hot electron phenomenon with photon excitations has been limited to excitation with photon energies below the ionization threshold and, therefore, to excitation energies provided by absorption of several and often a large number of photons. It is not a priori clear whether a single photon can cause the creation of the hot electron phase. Clearly, the competing direct ionization (spectroscopic) channel also appears prominently. For a recent such relatively low photon energy study of C_{60} , see [26]. However, in [17] it was shown that the absorption of single high energy photons by C_{60} can indeed give rise to hot electron emission, in parallel with the direct ionization of standard spectroscopic nature. The experimental signatures used to establish this were the ones associated with hot electron emission known from the multi-photon experiments and listed above, supplemented by the appearance energies of the fragmented ion at photon energies far above the ionization energy. The present experiment aimed to explore if and how these results applied also to C_{70} .

EXPERIMENTAL AND THEORETICAL PROCEDURES AND RESULTS

The experiments were performed at the GasPhase beamline at the synchrotron ring Elettra. The procedures were similar to those used for C_{60} [17] and only a brief description will be given here. For further specifics of the beam line the reader is referred to [27, 28]. The fullerene material was acquired from Sigma Aldrich, with a purity of 98 %. The sample was heated in situ for five days above 200 °C to out-gas solvents and other volatile contaminants. During measurements the molecules were sublimed from an oven with a temperature of initially 430 °C, slowly increasing to 470 °C at the end of the run, in order to keep the evaporation rate constant. The temperature was measured by a thermocouple attached to the oven. The linearly polarized light was filtered by standard filters at the different wavelengths as needed.

The electron spectra were recorded on single-count basis with a VMI spectrometer equipped with a dual delay line position sensitive detector and analyzed off-line. The coincidence of electrons and ions was extracted offline from the recorded time of flight of the ions with a electron detection

defining zero time. The detector only allowed detection of a single electron per event. To reduce the amount of false coincidences, the light intensity was reduced to electron count rates of 11–18 kHz and ion count rates of 2–8 kHz. As the detection efficiency does not depend on the origin of an electron, the spectra of molecules with a specific charge state are equal weight average spectra of all emitting charge states leading to the final state.

Spectra were recorded for the photon energies 16, 20, 22, 23.8, 26, 28, 30, 35, 40, 45, 50, 55, 60, 65, and 70 eV, always with the polarization parallel to the VMI detector plane. No tails on the mass spectra that would indicate a thermionic emission from a completely equilibrated system were observed in this experiment. Likewise, the substantial fragmentation that accompany thermionic emission for fullerenes was absent in the C_{70} mass spectra recorded in this work, as in our previous work on C_{60} [17]. The raw data spectra for the three lowest measured charge states of the unfragmented molecule at several selected photon energies are shown in Fig. 1.

The measured VMI spectra are the momentum distributions of the emitted electrons projected on the detector plane. On the VMI detector surface the required spherical symmetry of the hot electrons corresponds to a circular symmetry. Figure 2 shows the angular symmetry at the low energy electrons and the contrast to the asymmetry for higher energy electrons for a spectrum recorded after exposure to 16 eV photons. At low photon energies, the spectrum contains a wide base with structures that can be identified as features of direct ionization and hence of spectroscopic nature. The intensity peaking at zero kinetic energy, together with the appearance of the circular symmetry of these parts of the spectra, indicates the emergence of the hot electron spectra. Indeed, for all photon energies the central, lowest energy part of the spectra showed no sign of a correlation of the intensity with the direction of the light polarization, indicative of the required symmetrical distributions.

With the chosen light polarization the complete 3D distributions are obtained from the VMI spectra by deconvolution. The deconvolution was done with the inverse Abel transform as implemented in the MEVIR software [29]. Deconvolution of the spectra requires that the entire spectrum is projected onto the VMI detector surface. The highest electron energy for which this is guaranteed was 23 eV for the VMI voltages used in the experiment. This limits the photon energies to below 23 eV + $E_{i,1}$ for the singly ionized species, with $E_{i,1}$ the first ionization energy. The value of $E_{i,1} = 7.4$ eV was measured in Ref. [30], making this limit equal to 30.4 eV. A conservative safety margin on the masking reduces the highest photon energy to 26 eV for the singly charged species.

As a check of the procedure, the value of the ionization energy can be inferred by tracing the position of the highest occupied molecular orbital (HOMO) level as a function of the photon energy. The four photon energies from 16 eV to 23.8 eV can be used for that purpose. Figure 3 shows the trace used to determine $E_{i,1}$ on the VMI spectra deconvoluted with the procedure which is explained in more detail below. The value

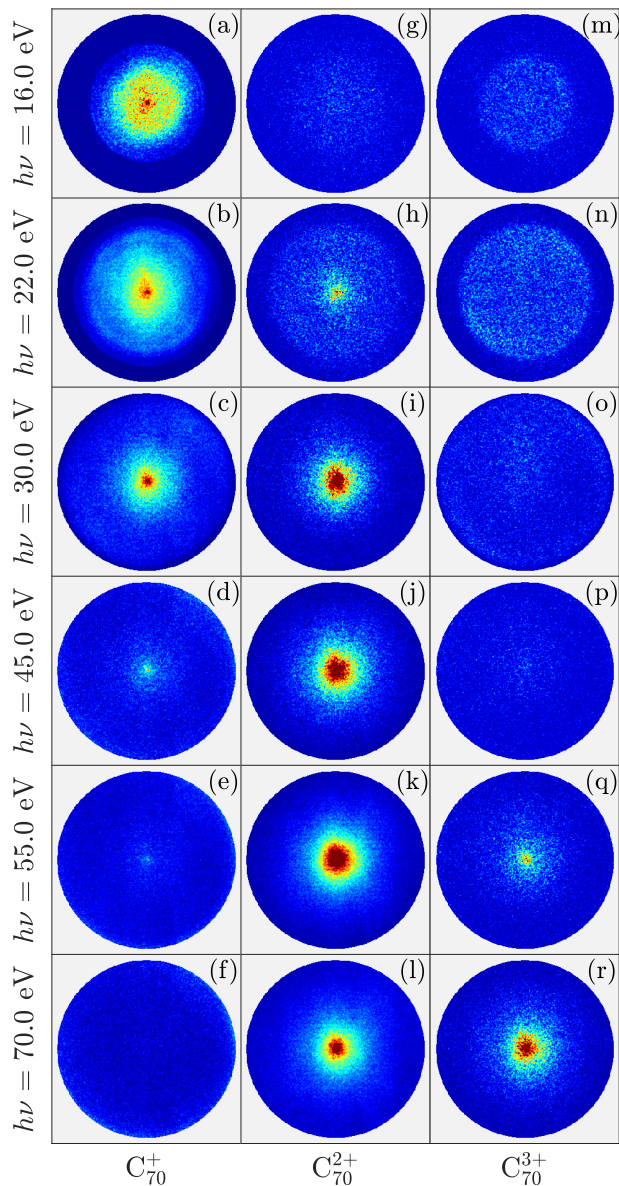


FIG. 1. The raw spectra of, from left to right, C_{70}^+ , C_{70}^{2+} , and C_{70}^{3+} . The narrowing of the intensity into a low momentum peak in the C_{70}^+ column results from the transformation of the ionization process from direct to hot electron emission. As seen, the second ionized species is first visible at 22 eV and the triply charged at 55 eV. The strong intensity of the highly charged species contrasts with the result for C_{60} , for which the high photon energy spectra are dominated by the fragments.

from this determination is 6.9 ± 0.5 eV, where the uncertainty is mainly due to the width of the peaks, i.e. consistent with the value from Ref. [30].

The electron detector can only assign a position and hence a transverse momentum to an event when it is hit by a single electron. As the detection efficiency is less than unity, it is therefore nevertheless still possible to detect spectra from double and triple ionization events. In these cases the spectra are sums of two spectra (for double ionization) or three spectra

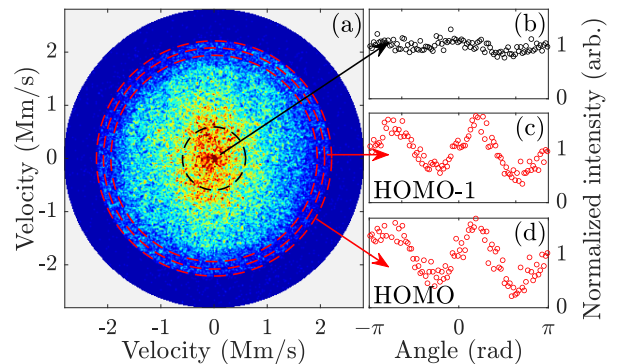


FIG. 2. A measured spectrum for C_{70} at photon energy 20 eV. Frame (a) shows electron intensities across the detector surface. Frame (b) shows the angular resolved intensities for the low energy part of the spectrum, and two high energy electron parts defined by the red circles are shown in frames (c,d). The flat distribution in frame (b) is consistent with a spherically symmetric momentum distribution, in contrast to the direct ionization electrons in frames (c,d).

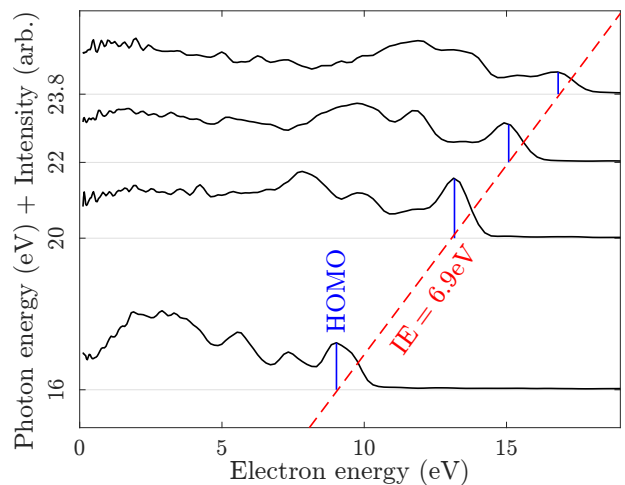


FIG. 3. The determination of the first ionization energy of C_{70} from the measured direct ionization spectra.

(for triple ionization) with equal weights. Since the detection limit is 21 eV and the sum of the two lowest ionization energies is 18.84 eV [31], all the electrons originating from double ionization events at photon energies below 40 eV are within detection range. For comparison, the value calculated with density functional theory for the second ionization energy is 10.3 eV (see below for the method used). With the calculated single ionization value of 7.3 eV this is in reasonable albeit not perfect agreement with the measured value. We have used the most conservative, experimental value. The appearance of the doubly charged ions at the photon energy $h\nu = 22$ eV is higher than the literature and theoretical values, as expected, and is consistent with the interpretation of the origin of the emitted electrons. In summary, inversion was performed for photon energies up to 26 eV for singly charged species and up to 40 eV for the doubly charged molecules, and for the latter

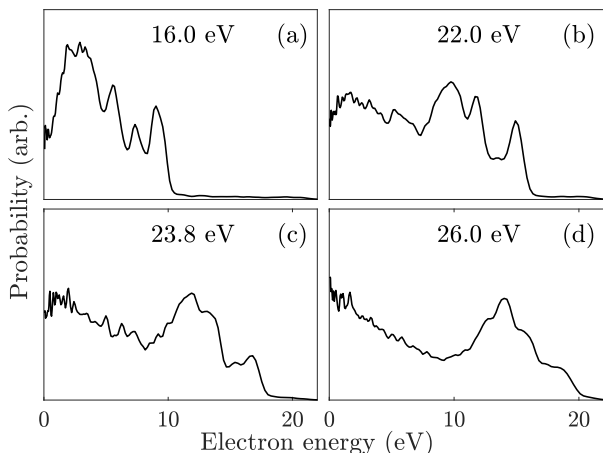


FIG. 4. The angular integrated electron spectra measured in coincidence with C_{70}^+ for a series of photon energies. The $h\nu$ spectrum is the highest measured spectrum that can be deconvoluted for singly ionized species. The direct ionization intensity, which for the $h\nu = 26$ eV spectrum is found between 10 and 20 eV, and the hot electron intensity, up to 10 eV, can be compared directly and are seen to be very similar at this photon energy.

only for single-electron events.

The spectroscopic nature of the high energy electrons is more apparent after deconvolution of the spectra. Figure 4, which shows deconvoluted spectra, demonstrates how this picture develops with increasing photon energy, in particular how the low energy electrons become increasingly intense. Figure 5 shows the spectra of single electrons detected in coincidence with doubly charged ions. The potential competing process of the low energy electrons by direct double ionization is not seen in the spectra in Fig. 5. These distributions would have a U-shape and the high energy end of such a spectrum would be present at the high kinetic energies, which is clearly not the case. We can therefore rule out this channel as a significant contribution also to the low energy part of the spectra.

Quantum chemical calculations of total and individual level energies were performed with density functional theory (DFT) on C_{70} using the ORCA 5.1 software package [32]. For this, the PBE functional [33] was used with the Def2-TZVPP basis [34], and included dispersion corrections via the D3BJ approximation [35]. The geometries of both molecules were optimized for the charge states 0, 1, 2 and all the electrons were included in the calculation. Moreover, vibrational frequencies were computed, confirming that structures represent true minima on the potential energy surface. In addition, single-point calculations of C_{60}^{q+1} and C_{70}^{q+1} on the optimized geometries of C_{60}^q and C_{70}^q were performed for $q = 0, 1, 2$, in order to calculate vertical first and second ionization energies.

Although the use of DFT to calculate the ionization energies and vibrational frequencies are well controlled, it is relevant to add a remark about the use of the single particle pseudo-states to calculate level densities. These do not in prin-

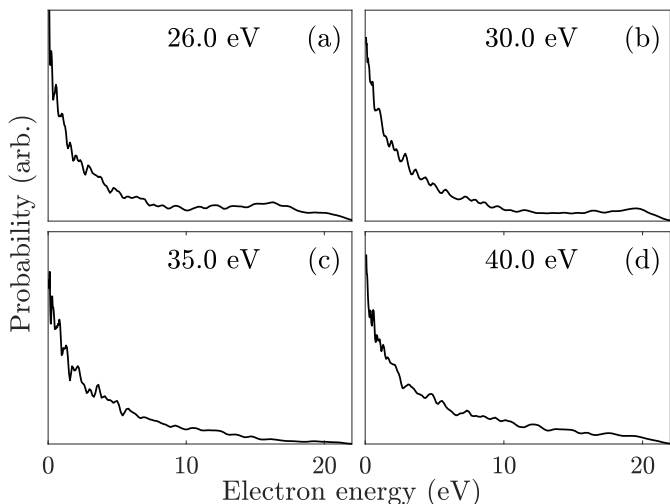


FIG. 5. The angular integrated electron spectra measured in coincidence with C_{70}^{2+} for the photon energies indicated in the frames.

ciple give the single particle states, and neither do they guarantee that the single particle approximation can be used. However, it is possible to compare level densities calculated with those states with the experimentally determined level density. The comparison was made in [13] where the two were found to agree very well. The only fit parameter used in that comparison was a single multiplicative constant which provided the absolute magnitude which can not be extracted from the experiments. We will therefore use the same procedure here to calculate the level densities.

ANALYSIS AND DISCUSSION

Before a quantitative analysis of the deconvoluted spectra is presented, it is of interest to consider the raw data plot in Fig. 1 in some detail. Important features of the processes here and for C_{60} (see Fig. 1 of [?] and Fig. 5 of [17]) are that *i*) the dominant open decay channel for the singly ionized C_{70} , shown in the second and third columns, is further electron emission producing the higher charge states of the molecules. For C_{60}^+ fragmentation is somewhat more pronounced. *ii*) intensities for C_{70}^{2+} (and for C) appear at lower photon energy than the fragments of C_{60}^+ , and *iii*) the difference in appearance energies of the triply and doubly ionized charge states of both C_{60} and C_{70} is much larger than the corresponding difference between the appearance energies of C_{58}^+ and C_{56}^+ from C_{60} .

Concerning *i*), the tendency to ionize twice instead of causing fragmentation was already reported in [36]. A similar effect has been seen in naphthalene [37], where the relative intensities of doubly ionized species relative to singly charged fragments increases when photon energies are changed from 20.4 eV to 29.8 eV, in parallel with a strong suppression of fragmentation processes at the higher energies.

The explanation of *ii*) is that the second ionization occurs from the hot electron ensemble, whereas the fragmentation of C_{60}^+ ions occurs from the completely vibrationally thermalized ion. The difference in the heat capacity of the two emitting systems accounts for the main part of this difference in appearance energies. These aspects have already been analyzed in detail in [13] and [17], where more quantitative details can be found. We note that also this observation is consistent with the hot electron ionization mechanism.

The reason for the behavior in point *iii*) is also the different nature of the decays of the two molecules. Addressing this question requires quantitative considerations of the appearance energies. For the C_{60} decay, the difference in the appearance energies of C_{58}^+ and C_{56}^+ is given mainly by the C_2 dissociation energy of C_{58}^+ . This is seen with the following simplified but still reasonably accurate calculation. The appearance energy for fragment m in a decay chain can be calculated as the photon energy which is the sum of the energies consumed in the previous decays plus the thermal energy needed for the m 'th decay. With an Arrhenius expression for the fragmentation rate constant we have

$$k(E) \sim \omega \exp(-D/T(E)), \quad (1)$$

with T being the effective microcanonical temperature at that energy E , and D the evaporative activation energy. A linear relation between the (microcanonical) vibrational temperature T and the excitation energy E is assumed (E_m^o is the energy offset in this curve, and k_B is set to unity):

$$E = C_k T - E_m^o. \quad (2)$$

With G defined as $\ln \omega t$ and t being the time of acceleration for the ion time-of-flight, this gives

$$h\nu_{\text{appear},m} \approx D_m \frac{C_m}{G} + E_m^o + \sum_{j=0}^{m-1} D_j - E_{\text{source}}. \quad (3)$$

The last terms in the equation accounts for the energy consumption in the prior decays and the initial energy of the molecule. The small amounts of energy carried away by the C_2 fragments are ignored in the expression. When the contribution $D_m C_m / G + E_m^o$ is approximately independent of m , the difference in the m 'th and the $m - 1$ 'th appearance energies is

$$h\nu_{\text{appear},m} - h\nu_{\text{appear},m-1} \approx D_{m-1}. \quad (4)$$

This approximate identity of the sequential differences between appearance energies hinges on the similarity of the emission activation energies and the constancy of the heat capacity. These are expected to hold to a decent approximation for the C_2 loss activation energy and for the vibrational thermal properties. For the hot electron emission processes seen for C_{70} , neither of these similarities will hold. The emission activation energies are the ionization energies, and their values increase with the charge state. Also the heat capacities vary with energy.

The estimate for the electron emission appearance energies goes as follows: The lowest effective temperature where hot electron emissions occur is determined by the combination of the electron-vibrational cooling time, which we will set to the C_{60} value of $\tau = 240$ fs [13] and the electron emission rate constant by the relation

$$k(E) = 1/\tau. \quad (5)$$

for smaller rate constants, dissipation into vibrational motion quenches the emission. The emission rate constant for electrons is also written as an Arrhenius expression where the activation energy is the ionization energy E_i . The frequency factor is denoted by ω_e . Although the value of ω_e depends on the charge state, the dependence is minor and beyond the precision here, and the factor will therefore be set to the neutral molecule value. To find the temperature we use the caloric curve for a Fermi gas,

$$E = \frac{1}{2} \alpha T^2. \quad (6)$$

The initial electronic energy from the source can be set to zero.

The photon energy at which the second ionized species appears can then be calculated with the same logic as for the unimolecular decays, i.e. adding the consumed energies of the previous decays to the excitation energy calculated by Eq. 5. The result is

$$h\nu_2 = \frac{\alpha}{2(\ln \omega_e \tau)^2} E_{i,2}^2 + E_{i,1} + \langle \varepsilon_{1,1} \rangle, \quad (7)$$

where $\langle \varepsilon_{1,1} \rangle$ is the average electron energy in the first ionization. By the same argument the triply ionized species appear at the photon energy

$$h\nu_3 = \frac{\alpha}{2(\ln \omega_e \tau)^2} E_{i,3}^2 + E_{i,1} + E_{i,2} + \langle \varepsilon_{2,1} \rangle + \langle \varepsilon_{2,2} \rangle, \quad (8)$$

where $\langle \varepsilon_{2,1} \rangle$ and $\langle \varepsilon_{2,2} \rangle$ are the electron energies of the first and second emitted electron in this process. These energies are larger than the counterpart for C_2 emission and can not be ignored in the analysis for electron emission. The emission of the first electron occurs at different energies for the two processes with the different final charge states, and $\langle \varepsilon_{1,1} \rangle$ is therefore different from (smaller than) $\langle \varepsilon_{2,1} \rangle$. With the value 26 eV for $h\nu_2$ (see Fig. 1), the first ionization energy $E_{i,1} = 7.4$ eV, and the second $E_{i,2} = 11.4$ eV, the coefficient in Eq.7 becomes

$$\frac{\alpha}{2(\ln \omega_e \tau)^2} = \frac{h\nu_2 - E_{i,1} - \langle \varepsilon_{1,1} \rangle}{E_{i,2}^2} = 0.13 \text{ eV}^{-1}, \quad (9)$$

when we use the value $\langle \varepsilon_{1,1} \rangle = 2$ eV. This result be compared below with the theoretical value derived from the rate constant after that calculation has been made.

Using the close similarity of the first two ionization energies to those of C_{60} , 7.6 eV and 11.4 eV, respectively, we adopt the third ionization energy of C_{60} , $E_{i,3} = 16.6$ eV, for C_{70} . This predicts an appearance photon energy of the third ionized molecule of

$$h\nu_3 = (18.8 + 5) \text{ eV} + 0.13 \text{ eV}^{-1} (16.6 \text{ eV})^2 = 60 \text{ eV} \quad (10)$$

where by inspection of the measured spectra shown in Fig. 5 we estimated the sum $\langle \varepsilon_{2,1} \rangle + \langle \varepsilon_{2,2} \rangle$ to be 5 eV. The estimated uncertainty on $h\nu_3$ is 9 eV. The experimental value of this cross-over photon energy is more uncertain than $h\nu_2$, but the above calculated value is within the range of the possible experimental values that lie between 45 eV and 60 eV.

For the above analysis a description in terms of a Fermi gas is sufficient, but for a more precise description and an assessment of the value of α , a more accurate calculation of the thermal properties of the hot electrons is required. The relevant thermal properties are the level densities, or density of states and the rate constants. They are calculated with the method given in the appendix of Ref. [13]. The input data are the energy levels from the DFT calculation of the energies. As the temperature is the microcanonical version we use the value derived from the level density ρ [20]

$$\frac{d \ln \rho(E)}{dE} = T^{-1}. \quad (11)$$

As k_B is set to unity, temperatures are therefore given in eV. This calculation for the singly charged molecule essentially confirms the Fermi gas Ansatz, albeit with an offset in the temperature. The fitted form is

$$E = \frac{1}{2} \alpha' (T^2 - T_0^2), \quad (12)$$

with $\alpha' = 46 \text{ eV}^{-1}$ and $T_0^2 = 0.3 \text{ eV}^2$. These values pertain to the singly charged molecule but the values for the other charge states are similar. As a side remark we note that the offset in the caloric curve is analogous to the similar and well documented offset that appears in the caloric curve of quantized vibrational motion. The interpretation of the offset here is different and the value can not be ascribed to a zero point motion as for the vibrations. The offset in temperature prevents a comparison of the α' fitted here and the α calculated from Eq. 9 with the rate constant in Eq. 13. This comparison will be made below.

The kinetic energy-resolved electron emission rate constant is given by the expression [13]

$$k^{(q)}(E, \varepsilon) d\varepsilon = \frac{2m_e \sigma(\varepsilon)}{\pi^2 \hbar^3} \varepsilon \frac{\rho^{(q+1)}(E - E_{i,q} - \varepsilon)}{\rho^{(q)}(E)} d\varepsilon \quad (13)$$

Here ε is the kinetic energy of the electron, m_e is the mass of the electron, $\rho^{(q)}(E)$ is the level density of charge state q at energy E , and $E_{i,q}$ is the ionization energy. The factor of two in Eq.13 is the spin degeneracy of the electron and $\sigma(\varepsilon)$ is the capture cross section for an electron in the Coulomb potential of the decay product. To find the relevant rate constant, the kinetic energy is integrated over:

$$k^{(q)}(E) \equiv \int_0^E k^{(q)}(E, \varepsilon) d\varepsilon. \quad (14)$$

The numerically integrated function is shown in Fig. 6.

With Eq. 13 we can describe the kinetic energy distributions with the function

$$P(\varepsilon; E, q) d\varepsilon = \sigma(\varepsilon) \varepsilon \rho^{(q+1)}(E - \varepsilon) d\varepsilon. \quad (15)$$

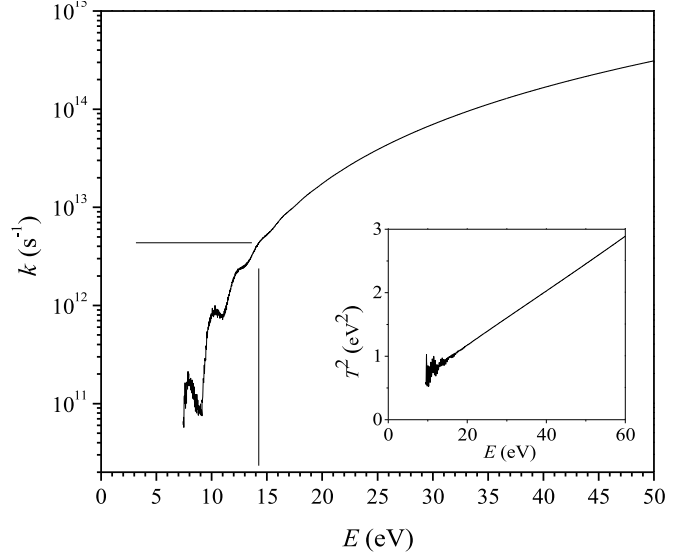


FIG. 6. The rate constant for emission of the second electron. The reciprocal coupling time and the corresponding lower limit of the energy of an emitting molecule are indicated by the horizontal and vertical lines. The inset shows the square of the microcanonical electron temperature vs. excitation energy. This is clearly very well represented by Eq. 12.

For the capture cross section the classical values used are

$$\sigma(\varepsilon) = \pi r_0^2 \left(1 - \frac{V(r_0)}{\varepsilon} \right), \quad (16)$$

and

$$V(r_0) = -\frac{(q+1)e^2}{4\pi\varepsilon_0 r_0} = -(q+1)3.0 \text{ eV}. \quad (17)$$

$r_0 = 5.3 \text{ \AA}$ is the (angle averaged) radius of the electron distribution in the molecule based on the bulk density of 1.64 g/cm^3 [38] and a FCC packing ratio of 0.74 [39]. The level densities can be approximated as

$$\rho^{(q+1)}(E - \varepsilon) \approx \rho^{(q+1)}(E) e^{-\varepsilon/T(E)}. \quad (18)$$

At a given photon energy the energies of the emitting ions are

$$E_1 = h\nu - E_{i,1} \quad (19)$$

for the first emitted electron, and

$$E_2 = h\nu - E_{i,1} - E_{i,2} - T(E_1), \quad (20)$$

for the second. $T(E_1)$ is the average value of the energy carried away by the electron during the first ionization. The temperatures are then found from Eq.12, which can be used for both charge states. Denoting these temperatures by T_1 and T_2 the spectra become

$$P(\varepsilon) \propto \frac{(\varepsilon + 3.0 \text{ eV}) e^{-\varepsilon/T_1}}{T_1 (T_1 + 3.0 \text{ eV})} + \frac{(\varepsilon + 6.0 \text{ eV}) e^{-\varepsilon/T_2}}{T_2 (T_2 + 6.0 \text{ eV})} \quad (21)$$

Given the fairly high temperatures, the term proportional to ε is needed here.

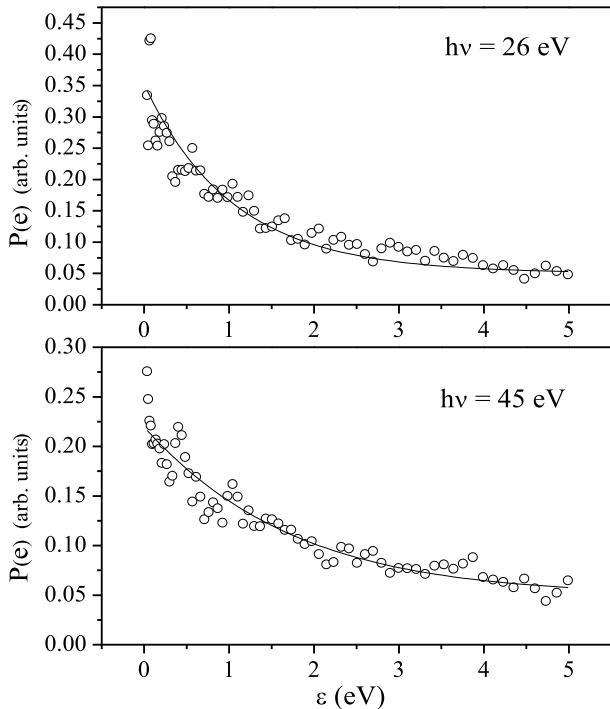


FIG. 7. The low energy parts of the experimental doubly ionized spectra (open circles) and the predicted bi-exponential decay in Eq.21 with the temperatures of 1.053, 0.753 eV for the $h\nu = 26$ eV curve, and 1.391, 1.174 eV for the $h\nu = 45$ eV curve, given by Eq.12 and calculated with the energies as described in the main text.

The two temperatures in Eq.21 are theoretically rather similar in the photon energy range 26 eV to 45 eV. The values of T_1 and T_2 for $h\nu = 26$ eV, for example, which gives rise to the largest difference, are 1.05 eV and 0.75 eV. For $h\nu = 45$ eV they are 1.39 eV and 1.17 eV. This makes a direct fit uncertain. A compounding complication for a fit is that the spectra are found to contain a small and broad background. Instead, the theoretical curves are plotted with a constant offset of 0.05. These are shown in Fig. 7 for the lowest and highest photon energies for spectra of doubly ionized molecules. The quality of the prediction for the spectra of the four photon energies not shown is very similar.

With the expression for the rate constant we check the consistency of the hot electron picture by a comparison of the theory value α' with the experimental value α on the right hand side of Eq. 9. The rate constant to choose is the one corresponding to the time constant of dissipation of the electronic excitation energy into vibrational motion, Eq.5; $k(E) = 1/240$ fs. This gives the energy 13 eV. Using this for the first ionization gives the corresponding singly ionized version of Eq. 9:

$$\frac{\alpha}{2(\ln \omega_e \tau)^2} = \frac{13\text{eV}}{E_{i,1}} = 0.10 \text{ eV}^{-1}, \quad (22)$$

which is in reasonable agreement with the experimental value

of 0.13 eV^{-1} . We take this as a confirmation of the values used. It should be noted that clearly this only confirms the product of the electron emission frequency factor and the value of τ and not the values of the two quantities separately.

Finally we will address the question of the initial excitation of the molecule. One of the challenges still facing the description of the phenomenon is an explanation of the mechanism of the initial excitation. A part of this question, which will be susceptible to future experiments and that has obvious implications for the kinetic energies of the emitted electrons, is the branching ratio between direct and hot electron ionization. A full quantum mechanical description of the dynamics of the process is beyond the scope of this publication, but we will suggest a possible mechanism which will convert a single-particle excitation into multi-electron excitation and hence provide the initial energy dissipation needed to produce the electron spectra seen in this work.

The suggested description builds on the single-electron picture. In the initial reaction, the photon is absorbed by a single electron which is promoted to a vacuum state, converting all energy in excess of the binding energy, E_b , to kinetic energy according to the standard relation

$$E_k = h\nu - E_b. \quad (23)$$

After this, the electron starts to move across the fullerene. The time it takes for this crossing is given classically by

$$t_c \sim \frac{2r_0}{\sqrt{2(h\nu - E_b)/m}}. \quad (24)$$

During this motion the remaining valence electrons will be exposed to the electric field of the excited electron. This will excite the surface plasmon resonance with some probability, which will depend on the speed of the emitted electron. Setting t_c to half the period of a resonance, the departing electron will then be in resonance with an excitation with a quantum energy of

$$\hbar\omega = \hbar\pi\sqrt{2(h\nu - E_b)/m}/2r_0. \quad (25)$$

A kinetic energy of 50 eV, for example, will give the value of 8.6 eV for the right hand side, and be optimal for exciting an oscillation around that energy. This energy is on the order of the peak energy of the surface plasmon resonance, which is located with a centroid energy of $\hbar\omega \approx 20$ eV and, significantly, with a width of similar magnitude [40]. Electron energy loss spectroscopy shows a strong absorption of collective nature from 5 eV electron energy and up [41], similar to the optical cross section. The attenuation length was given for C_{60} films in [42], for a single energy. The value compares well with values from intercalated fullerite samples and the pure fullerite attenuation length at the energies relevant here can be taken with some confidence to be around the size of the molecule. There is little reason to believe that the value for C_{70} is significantly different, given the similar spectra in [41]. These experimental indications suggest that excitation by the prescribed mechanism is indeed likely to occur.

Leaving aside the precise value of the matrix element for exciting the plasmon resonance, it is also clear that at least the time scales match semiclassically. Moreover, as this resonance is a collective motion of a large number of electrons, with the number reflected in the large oscillator strength, a coupling to it will deposit the kinetic energy into a large number of valence electrons, facilitating the dissipation into incoherent energy which is the hallmarks of the hot electron phase.

The mechanism suggested here has some support in the ionization of metal clusters. In Ref.[43] ionization yields of alkali metal clusters are reported. The data show reductions in ionization yields above the surface plasmon resonance. This is discussed qualitatively in terms of a mechanism that couple photo-electrons and the plasmon, similar to the one predicted here. In particular, it will impact measured ionization cross sections, such as those reported in Ref. [40], although for those measurements the corrections will mainly occur at the high energy side of the peak value. An experimental signature of the effect is a reduced direct ionization efficiency and an increased amount of hot electron ionization in the energy region where the kinetic energy in the initial stage is conducive to excitation of the resonance, i.e. fulfills Eq.25. This is effectively a shadow of the plasmon resonance. This Resonance Ionization Shadowing must be expected to be present in other clusters or molecules that have large oscillator strength resonances. The precise parameters of the effect, such as the branching ratio of direct ionization to hot electron formation, will depend on the centroid energy, its width and to some extent also on its oscillator strength. The molecular geometry may likewise determine the initial coupling to the resonance.

CONCLUSION AND OUTLOOK

We have measured the single photon hot electron ionization of C_{70} . It shows the same main features as the process for C_{60} , albeit with a somewhat stronger intensity of the doubly ionized species compared to fragmentation. The measurements thus demonstrate that the mechanism is not restricted to a single fullerene. The mechanism by which the molecules absorb a photon with energy above the ionization energy and equilibrates it is not yet established. In this work we have suggested a mechanism involving excitation of the surface plasmon by a departing electron. This mechanism should be fairly general. If correct, it will give a suppression of the ionization as a function of photon energy in a wide energy region, usually above the plasmon centroid. Part of the suppression will be compensated by the enhanced hot electron emission. The suggested mechanism is not a direct excitation of the plasmon and explains that the onset of the hot electron emission appears above its centroid energy, as already seen for C_{60} . Hence, contrary to previous statements, the surface plasmon is relevant after all, albeit only indirectly.

ACKNOWLEDGEMENT

KH acknowledges support from NSFC with grant No. 12047501, from the 111 Project of the Ministry of Science and Technology of People's Republic of China' under grant no. B20063, and Y. Gong for advice on the presentation. P.F. acknowledges the Research Foundation Flanders (FWO) for a Senior postdoctoral grant. The computational resources and services used in this work were provided by the VSC (Flemish Supercomputer Center), funded by the FWO and the Flemish Government. We acknowledge Elettra Sincrotrone Trieste for providing access to its synchrotron radiation facilities. The authors also acknowledge the open access contribution of the Research Infrastructure (RI) Elettra. Comments from V. Kresin are gratefully acknowledged.

* hansen@lzu.edu.cn, KlavsHansen@tju.edu.cn

† vitali.zhaunerchyk@physics.gu.se

- [1] S. I. Anisimov, B. L. Kapeliovich, and T. L. Perel'man, *Sov. Phys. JETP* **39**, 375 (1974).
- [2] J. M. Weber, K. Hansen, M. W. Ruf, and H. Hotop, *Chem. Phys.* **239**, 271 (1998).
- [3] E. E. B. Campbell, K. Hansen, K. Hoffmann, G. Korn, M. Tchapyguine, M. Wittmann, and I. V. Hertel, *Phys. Rev. Lett.* **84**, 2128 (2000).
- [4] R. Schlipper, R. Kusche, B. v. Issendorff, and H. Haberland, *Appl. Phys. A* **72**, 255 (2001).
- [5] M. Maier, M. Schätzel, G. Wrigge, M. Astruc Hoffmann, P. Didier, and B. v. Issendorff, *Int. J. Mass Spectrom.* **252**, 157 (2006).
- [6] M. Maier, G. Wrigge, M. Astruc Hoffmann, P. Didier, and B. v. Issendorff, *Phys. Rev. Lett.* **96**, 117405 (2006).
- [7] M. Kjellberg, O. Johansson, F. Jonsson, A. V. Bulgakov, C. Bordas, E. E. B. Campbell, and K. Hansen, *Phys. Rev. A* **81**, 023202 (2010).
- [8] M. Kjellberg, A. V. Bulgakov, M. Goto, O. Johansson, and K. Hansen, *J. Chem. Phys.* **133**, 074308 (2010).
- [9] V. V. Flambaum, A. A. Gribakina, G. F. Gribakin, and C. Harabati, *Phys. Rev. A* **66**, 012713 (2002).
- [10] G. Gribakin and S. Sahoo, *Journal of Physics B: Atomic Molecular and Optical Physics* **36**, 3349 (2003).
- [11] J. Heraud, M. Vincendon, P.-G. Reinhard, P. M. Dinh, and E. Suraud, *Eur. Phys. J. D* **75** (2021).
- [12] E. E. B. Campbell, K. Hansen, M. Hedén, M. Kjellberg, and A. V. Bulgakov, *Photochem. Photobiol. Sci.* **5**, 1183 (2006).
- [13] K. Hansen, K. Hoffmann, and E. E. B. Campbell, *J. Chem. Phys.* **119**, 2513 (2003).
- [14] V. Schettino, M. Pagliai, L. Ciabini, and G. Cardini, *J. Phys. Chem. A* **105**, 11192 (2001).
- [15] D. Mongin, P. Maioli, J. Burgin, P. Langot, E. Cottancin, S. D'Addato, B. Canut, M. Treguer, A. Crut, F. Vallée, et al., *J. Phys. Condens. Matter* **31**, 084001 (2019).
- [16] W. Cong-fang, A. Xi-cheng, X. Zong-ju, and Z. Ying-hua, *Chinese Phys. Lett.* **13**, 668 (1996).
- [17] K. Hansen, R. Richter, M. Alagia, S. Stranges, L. Schio, P. Salén, V. Yatsyna, R. Feifel, and V. Zhaunerchyk, *Phys. Rev. Lett.* **118**, 103001 (2017).
- [18] E. Herbst, *Journal of Physics: Conference Series* **4**, 17 (2005).

- [19] J. U. Andersen, E. Bonderup, and K. Hansen, *J. Phys. B* **35**, R1 (2002).
- [20] J. U. Andersen, E. Bonderup, and K. Hansen, *J. Chem. Phys.* **114**, 6518 (2001).
- [21] K. Hansen, *Statistical Physics of Nanoparticles in the Gas Phase*, vol. 73 of *Springer Series on Atomic, Optical, and Plasma Physics* (Springer, Dordrecht, 2018).
- [22] F. Lépine and C. Bordas, *Phys. Rev. A* **69**, 053201 (2004).
- [23] G. Walder and O. Echt, *Int. J. Modern Physics B* **6**, 3881 (1992).
- [24] J. Andersson, S. Zagorodskikh, A. H. Roos, O. Talae, R. J. Squibb, D. Koulentianos, M. Wallner, V. Zhaunerchyk, R. Singh, J. H. D. Eland, et al., *Sci. Rep.* **9**, 17883 (2019).
- [25] A. Lassesson, K. Hansen, M. Jönsson, A. Gromov, E. Campbell, M. Boyle, D. Pop, C. P. Schulz, I. V. Hertel, A. Taninaka, et al., *Eur. Phys. J. D* **34**, 205 (2005).
- [26] H. R. Hrodmarsson, G. A. Garcia, H. Linnartz, and L. Nahom, *Phys. Chem. Chem. Phys.* **22**, 13880 (2020).
- [27] R. R. Blyth, R. Delaunay, M. Zitnik, J. Krempasky, R. Krem-paska, J. Slezak, K. C. Prince, R. Richter, M. Vondracek, R. Camilloni, et al., *J. Electron Spectrosc. Relat. Phenom.* **101-103**, 959 (1999).
- [28] P. O’Keeffe, P. Bolognesi, M. Coreno, A. Moise, R. Richter, G. Cautero, L. Stebel, R. Sergo, L. Pravica, Y. Ovcharenko, et al., *Rev. Sci. Instrum.* **82**, 033109 (2011).
- [29] B. Dick, *Phys. Chem. Chem. Phys.* **16**, 570 (2014).
- [30] O. V. Boltalina, I. N. Ioffe, L. N. Sidorov, G. Seifert, , and K. Vi- etze, *J. Am. Chem. Soc.* **122**, 9745 (2000).
- [31] H. Steger, J. de Vries, B. Kamke, W. Kamke, and T. Drewello, *Chem. Phys. Lett.* **194** (1992).
- [32] F. Neese, F. Wennmohs, U. Becker, and C. Riplinger, *J. Chem. Phys.* **152**, 224108 (2020).
- [33] B. Hammer, L. B. Hansen, and J. K. Nørskov, *Phys. Rev. B* **59**, 7413 (1999).
- [34] F. Weigend and R. Ahlrichs, *Phys. Chem. Chem. Phys.* **7**, 3297 (2005).
- [35] S. Grimme, S. Ehrlich, and L. Goerigk, *J. Comput.* **32**, 1456 (2011).
- [36] K. Mitsuke, H. Katayanagi, B. P. Kaffle, C. Huang, H. Yagi, M. S. I. Prodhon, and Y. Kubozono, *J. Phys. Chem. A* **111**, 8336 (2007).
- [37] G. Reitsma, J. Hummert, J. Dura, V. Lorient, M. J. J. Vrakking, F. L. pine, and O. Kornilov, *J. Phys. Chem. A* **123**, 3068 (2019).
- [38] A. A. Kolomenskii, M. Szabadi, and P. Hess, *App. Surf. Sci.* **86**, 591 (1995).
- [39] N. W. Ashcroft and N. D. Mermin, *Solid State Physics* (Saunders College Publishing, 1976).
- [40] I. V. Hertel, H. Steger, J. de Vries, B. Weisser, C. Menzel, B. Kamke, and W. Kamke, *Phys. Rev. Lett.* **68** (1992).
- [41] E. Sohmen, J. Fink, and W. Krätschmer, *Z. Phys. B* **86**, 87 (1992).
- [42] H.-N. Li, X.-X. Wang, and W.-F. Ding, *J. Electron Spectros. Relat. Phenomena* **153**, 96 (2006).
- [43] K. Wong, V. Kasperovich, G. Tikhonov, and V. V. Kresin, *Appl. Phys. B* **73**, 407 (2001).